Paper No. C2

DYNAMIC STALL CONTROL BY AIRFOIL DEFORMATION

W.GEISSLER, M.RAFFEL

DEUTSCHE FORSCHUNGSANSTALT FÜR LUFT- UND RAUMFAHRT,
GÖTTINGEN, GERMANY

September 14-16, 1993

CERNOBBIO (COMO)

ITALY

Dynamic Stall Control by Airfoil Deformation

by

W.Geissler,M.Raffel

Abstract

*With combined numerical and experimental investigations of the dynamic stall process on retreating helicopter rotor blades new insight into the complex unsteady flows involved have been achieved recently. With these new experiences in mind it is of increasing interest to suitably **influence** the flow, i.e. by dynamic airfoil deformation. The present paper describes first steps towards an improvement of the dynamic stall effects with respect to the time-dependent flows and overall forces by both numerical and experimental tools.*

1.Introduction.

The unsteady and separating flow on a retreating helicopter rotor blade at high forward speed flight limits the maximum speed of the flight-vehicle and may even lead to dangerous stall flutter. On the one side numerical methods based on the two-dimensional, time-accurate Navier-Stokes equations [1],[2] have been developed to calculate these flows. On the other side new non-intrusive diagnostic techniques like interferometry [3] and particle image velocimetry (PIV), [4] have been improved and recently applied successfully to measure instantaneous density and velocity fields about oscillating models.

These efforts gained new insight into the complex unsteady separating flows involved. It has been shown in [5] that compressibility effects may play a key-role in the initiation and shedding of the dynamic stall vortex.

In the present paper first steps are carried out towards suitably influence the dynamic stall process by dynamically controlled airfoil deformations. The idea to influence these flows is not new.

- With a leading edge slat [6] the dynamic stall vortex could almost be eliminated and the negative peak of the pitching moment could be avoided.

- With blowing [7] the dynamic stall effects could be reduced and the performance of the airfoil was improved significantly

However in these cases the improvements on the one side were mainly compensated by negative effects (additional drag of the slat-system, additional power for blowing, etc) on the other side.

The present study follows a different strategy: The airfoil is allowed to **deform** its shape dynamically during the oscillatory motion. This strategy has the advantage to improve some positive effects of the dynamic stall process. i.e. increase the maximum lift and simultaneously reduce some negative effects. i.e. shift the drag-rise and moment-stall events to higher incidences or even reduce or avoid them.

The present paper gives results of some systematic numerical investigations of the flows about deforming airfoils including a visualization of the flow by some video movie sequences. In addition first results of experimental flow field investigations about a deformable airfoil model using particle image velocimetry (PIV) will be discussed and compared with the numerical data.

2. Numerical investigations.

The flows under investigation are characterized by viscous and unsteady effects with limited regions where compressibility effects are important as well. Due to the shedding of concentrated vortices viscous effects are not confined to the airfoil boundary layer. These flow complexities make it necessary to base the numerical code on the complete equations, i.e. the Navier-Stokes equations. The calculations have to be carried out in a time-accurate manner. The computing times even in the present 2d-case are therefore large.

2.1 Navier-Stokes code

The numerical method to solve the time-dependent 2d-Navier-Stokes equations for accelerated moving (oscillating) airfoils has been described in detail in [2],[5]. The approximate factorization implicit method of Beam and Warming [8] has been applied using central differencing for the spatial derivatives. Special eigenvalue-scaled numerical damping terms have been added to sufficiently control the stability of the code. The simple algebraic turbulence model of Baldwin and Lomax has been used throughout these investigations.

2.2 Dynamic mesh deformation.

A special feature of the present numerical code is the treatment of the curvilinear coordinate mesh used in the calculations. The mesh is fixed to the moving airfoil as well as to the space-fixed outer boundary: So in the considered space-fixed frame of reference the mesh is allowed to deform dynamically. This feature is important because it also allows to treat cases where the airfoil is oscillating (i.e. in pitching mode) and in addition changing its shape dynamically. To avoid excessive increases of computing times the mesh is only calculated numerically at special time points which are prescribed by the deformation strategy (section 2.3). At arbitrary times the mesh is calculated simply by an interpolation procedure.
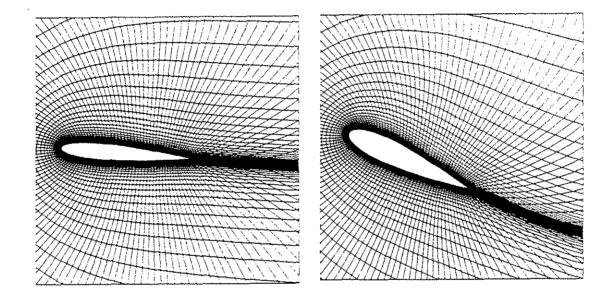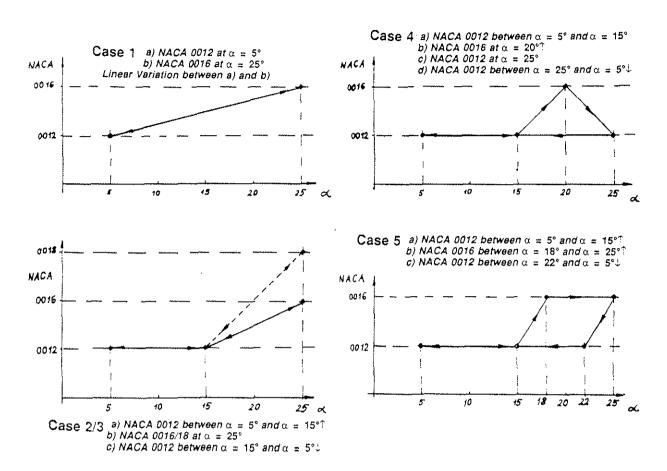

Fig.1: Calculated mesh in extreme incidence positions.
NACA0012 at α = 5° (left), NACA0018 at α = 25° (right)

In the present study a linear interpolation procedure with respect to incidence is used. Other interpolation rules are possible but have not yet been treated. *Fig.1* shows two meshes in the extreme incidence positions of the pitching oscillation about the quarter chord: α = 5° / 25° with NACA0012 at α = 5° (left) and NACA0018 at α = 25° (right). During oscillation between these extreme incidences the airfoil is smoothly changing its shape.

The airfoil deformations are applied to influence dynamic stall characteristics of the retreating rotor blade. It has been shown in [5] that compressibility effects in form of a small supersonic bubble occur at the airfoils leading edge during upstroke. This bubble initiates the dynamic stall process. It is the aim of this study to avoid or at least shift the supersonic bubble to higher incidences. This will be accomplished by a thickening of the airfoil during its upstroke motion with a reduction of the curvature within the nose region

For the numerical calculations the interpolation rule for the deforming mesh is related to the highly changing *incidence* of the airfoil. This procedure seems suitable because the important events of dynamic stall like begin of vortex shedding. lift- and moment-stall, etc. are preferably related to the

instantaneous incidence during up/down-stroke of the airfoil rather than to the instant of time or phase of the oscillatory motion.

Case 1 a) NACA 0012 at α = 5°
         b) NACA 0016 at α = 25°
         Linear Variation between a) and b)

Case 4 a) NACA 0012 between α = 5° and α = 15°
         b) NACA 0016 at α = 20°↑
         c) NACA 0012 at α = 25°
         d) NACA 0012 between α = 25° and α = 5°↓

Case 2/3 a) NACA 0012 between α = 5° and α = 15°↑
           b) NACA 0016/18 at α = 25°
           c) NACA 0012 between α = 15° and α = 5°↓

Case 5 a) NACA 0012 between α = 5° and α = 15°↑
         b) NACA 0016 between α = 18° and α = 25°↑
         c) NACA 0012 between α = 22° and α = 5°↓

Fig.2: Deformation strategies.

Several deformation strategies have been used for calculation and their influences on the overall forces and moment as well as on the development of the flow-fields have been studied in detail. Fig.2 shows the five different cases which have been treated each with the incidence variation:

$$\alpha = 15° + 10° \sin \omega^* T \qquad (1)$$

and the parameters:

$$\omega^* = \frac{2\pi f c}{U_\infty} = 0.3 \,, Ma = 0.28 \,, Re = 3 \cdot 10^6 \qquad (2)$$

In case 1 the airfoil changes its shape from α = 5° to α = 25° between NACA0012 and NACA0016.

In case 2 the NACA0012 airfoil shape is kept unchanged between 5° ≤ α ≤ 15° and changed between 15° < α ≤ 25° between NACA0012 and NACA0016 or in case 3 between NACA0012 and NACA0018.

Case 4 includes a case where NACA0012 is again kept unchanged between α = 5° and α = 15° but thickens its shape between α = 15° and α = 20° upstroke to NACA0016 and reduces its thickness again between α = 20° and α = 25° upstroke. In the whole downstroke phase the airfoil is again NACA0012 unchanged. In this case the airfoil thickening is limited to a short period during upstroke.

Case 5 finally shows a complete loop of airfoil deformation within the higher incidence regime.

For the interpolation procedure mentioned above coordinate meshes have only been calculated at *edge-points* of the deformation loops. In case 1 only two meshes have to be calculated: at $\alpha = 5°$ (NACA0012) and at $\alpha = 25°$ (NACA0016). In case 2/3 three meshes must be calculated: at $\alpha = 5° / 15°$ (NACA0012) and at $\alpha = 25°$ (NACA0016/18). Corresponding more meshes are necessary in case 4 (4 meshes) and case 5 (5 meshes).
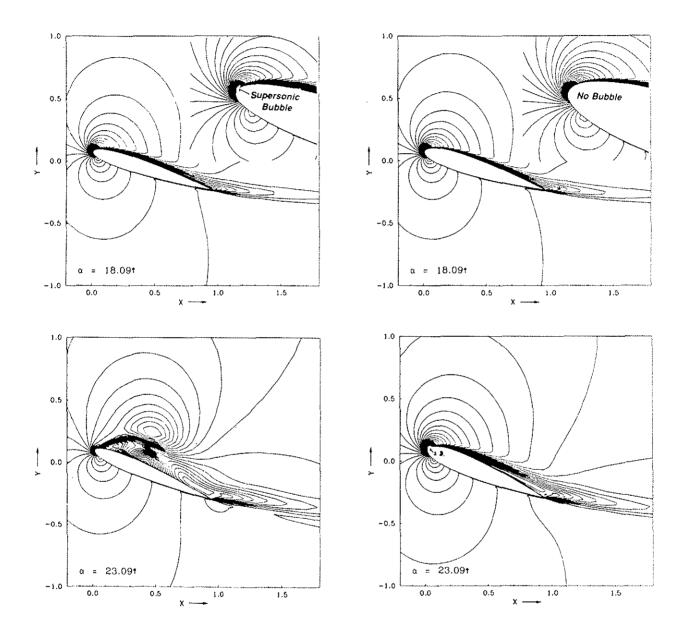

Fig.3: Machnumber contours.
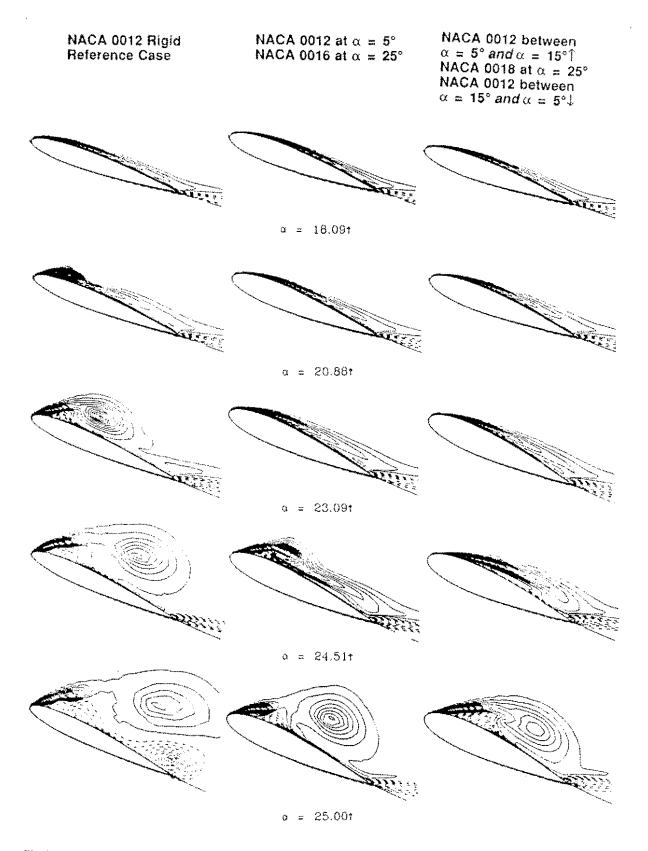**NACA0012 rigid (left), NACA0012-0016 (case 1) (right).**

NACA 0012 Rigid
Reference Case

NACA 0012 at $\alpha = 5°$
NACA 0016 at $\alpha = 25°$

NACA 0012 between
$\alpha = 5°$ and $\alpha = 15°\uparrow$
NACA 0018 at $\alpha = 25°$
NACA 0012 between
$\alpha = 15°$ and $\alpha = 5°\downarrow$

$\alpha = 18.09\uparrow$

$\alpha = 20.88\uparrow$

$\alpha = 23.09\uparrow$

$\alpha = 24.51\uparrow$

$\alpha = 25.00\uparrow$

Fig.4: Vorticity distributions on deforming airfoils.

2.3 Results.

The deformation cases discussed in the previous section have been used for numerically calculating the flowfields with the incidence variation (1) and the set of parameters (2). This is assumed a deep dynamic stall case with severe vortex shedding and a locally embedded supersonic bubble.

Fig.3 shows Machnumber contours for two instantaneous incidences (α = 18.09°, 23.09°) during upstroke. For the rigid NACA0012 airfoil reference case the supersonic bubble is detected at α = 18.09°↑ which is not found in the deforming case 1 at the same incidence. At α = 23.09°↑ the dynamic stall process has already been started with shedding of a concentrated vortex in the rigid case whereas in the deforming case the flow is still attached. However if one looks into the details of the leading edge flow, a supersonic bubble is also developing on the deforming airfoil but to a later time (higher incidence).

Fig.4 shows vorticity contours for the three cases: rigid / case 1 / case 3 during the upstroke motion of the airfoil. In the rigid case the vortex formation starts already at about α = 20°↑. In the two deforming cases no sign of separation is visible. At α = 23°↑ the dynamic stall vortex has already been fully developed in the rigid case whereas the two deforming cases still do not show any sign of vortex formation. At α = 24.5°↑ the vortex has already traveled half the airfoil chord in the rigid case. The smoothly deforming airfoil (case 1, middle figures) shows first concentration of vorticity at the leading edge. In case 3 (right hand figures) the flow is still attached. At the maximum incidence (α = 25°) the vortex has already been separated from the airfoil in the rigid case and a counter-rotating vortex is developing at the trailing edge. In both deforming cases the vortex is still attached to the airfoil surface.

These flow behaviors for the different deformation cases have a severe impact on the overall lift-, drag- and pitching-moment distributions as is displayed in *Fig.5*. Hysteresis loops of forces and moment with respect to incidence are shown and compared with the NACA0012 rigid case (dashed curves). In both cases (1,2) the lift-stall has slightly been shifted to a higher incidence. In the post-stall (down-stroke) regime the hysteresis loop in lift is changed considerably: the lift remains on a higher level and reaches attached values at earlier times as the rigid case.

The drag-curves show in the deforming case a severe shift of the drag rise to higher incidences. A similar behavior can be observed for the moment-stall: The steep decrease of the pitching moment (nose-down moment) is also shifted from about α = 20°↑ in the rigid case to α = 23°↑ in the deforming airfoil case (case 1). Here it must be pointed out that the areas between the moment curves are a measure of the aerodynamic damping and the direction of traversing these curves indicates whether the case is aerodynamically damped or undamped. Due to a shift of moment-stall to about α = 23°↑ a hysteresis loop is formed (case 1, left hand figure) which signals negative damping (see shaded area). This effect is mainly suppressed in deformation case 2 (right hand figure) but both cases show still a strong negative (nose-down) peak of the pitching moment

Drag rise and shift of moment-stall can also be observed in deformation case 4 (Fig 2) where only a short term deformation during upstroke is verified (between α = 15° and α = 25°, with a peak thickness at α = 20°). In this case the post-stall behavior is very similar compared to the rigid airfoil case.

Case 5 finally (not displayed) shows a similar behavior as case 1: Beside of a favorable shift of drag-rise and moment-stall events to higher incidences a considerable amount of negative damping is created as well.

The results show that the influence of dynamic stall characteristics by dynamic airfoil deformation can be of remarkable benefit but does not always lead to a complete success. The reason for this is the application of *prescribed* deformation rules which should be assumed as a first step towards a more rigorous solution of a *design problem*, i.e. to change the slope of the airfoil dynamically in such a way that a supersonic bubble is completely avoided. These goals remain to be solved in the future.
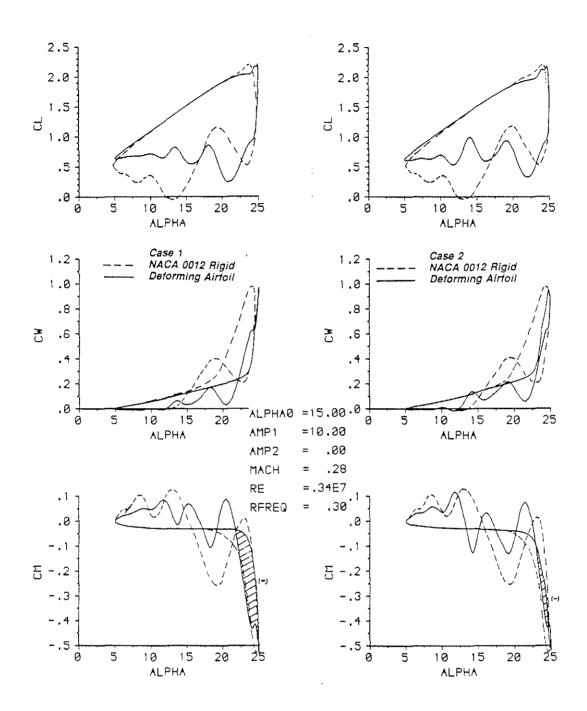
Fig.5: Hysteresis loops of lift-, drag- and pitching- moment-distributions as functions of incidence.

3. Experimental investigations.

The numerical results discussed so far give already important insights into the possibilities how to influence dynamic stall by airfoil deformation. However it is a different and complicated task to
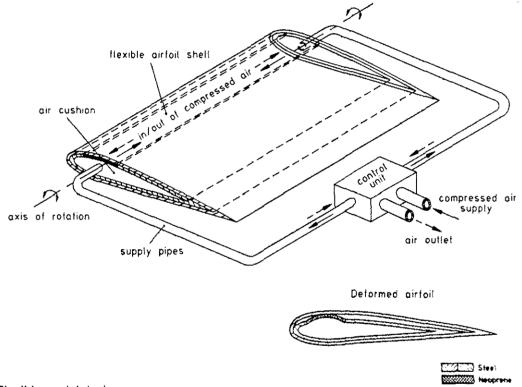
verify such a deformation at least in a wind-tunnel test. Different strategies are possible to solve the problem by
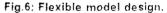
- deformations by mechanical means

- pneumatic deformations

- application of smart materials

In a preliminary study a 2d-wind-tunnel model has been designed to achieve the dynamic airfoil deformation by a *pneumatic* device.

3.1 Flexible model design.

To investigate flowfields under deep dynamic stall conditions corresponding severe incidence variations with amplitudes up to $n = 10°$ in combination with oscillation frequencies of up to 10 Hz have to be realized. Adding additional structures inside the model (i.e. actuators) to achieve the deformation mechanically means additional inertia forces and thus limitation of the frequency range. A *pneumatic* device as sketched in *Fig.6* has considerable advantages: No additional weight has to be added inside the model. Pressure supplies are already available at wind-tunnel facilities.

Fig.6: Flexible model design.

The present model consists of a flexible shell which forms the datum airfoil shape (NACA0012). Inside this shell a deformable *air-cushion* is placed (Fig.6) which is connected to the compressed air-supply via pipes and a control unit. The control unit allows the dynamic compression and decompression of the air-cushion with a frequency and phase directly connected to the pitching oscillation of the model.

A part of the air-cushion (see detail in Fig 6) is cutted out and closed by a neoprene diaphragm at the leading edge upper surface of the airfoil. Due to the much larger flexibility of the neoprene sheet the airfoil leading edge region can be thickened without too much effecting the remainder of the airfoil model. In compressed condition a thickening of the airfoils leading edge to approximately NACA0016 has been achieved. Due to the flexibility of the outer shell the model reduces its shape back to NACA0012 if the pressure inside the air-cushion is reduced.

3.2 Laboratory test.

The flexible model described in the previous section was first investigated in a functional test. The movement of the flexible shell was measured by a displacement pick up at one position ($x/c = 0.15$) on the upper surface. *Fig.7a* shows the time dependent displacement as measured by the pick up. A displacement of about 4.2mm has been achieved with a pressure difference of 1 bar from the pressure supply. The deformation frequency was adjusted to 6.6Hz corresponding to the pitching oscillation frequency of the model in the ISL-windtunnel test. *Fig.7b* displays the airfoil shapes in the undeformed and maximum deformed stages as detected by a video camera combined with a stroboscopic light source. It has already been pointed out in section 3.1 that the air-cushion should deform only the upper surface of the airfoil leaving the other parts nearly unchanged. Fig.7b shows that this goal has been realized in good approximation.
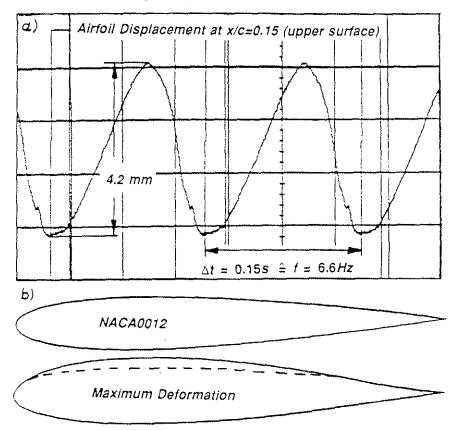

Fig.7:
a) Displacement distribution from pick up.
b) Achieved airfoil deformation.

3.3 Windtunnel tests on oscillating models using PIV.

For the investigation of unsteady flowfields about oscillating airfoil models the experimental set up of the French-German Institute St. Louis, France (ISL) has been used within a joint effort between DLR and ISL. The test set up is described in detail in [9]. In the low speed ISL windtunnel a maximum airspeed of about 35 m/s could be achieved. With the driving mechanism for the airfoil models a maximum frequency in pitching motion of nearly 10Hz could be realized with maximum amplitudes of about 10°. To get comparable results with the numerical data a reduced frequency $\omega^* = 0.3$ was prescribed and realized with f = 6.6Hz oscillation frequency and $U_\infty = 28m/s$ mainflow velocity (model chord c = 0.2m).

However due to the low speed conditions the flow is assumed to be subsonic during the whole oscillatory cycle. i.e. compressibility effects could not be studied during the present tests.
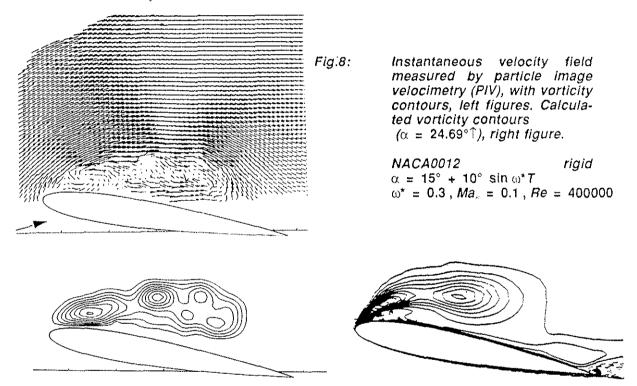
On the other hand the Reynoldsnumber was only about Re = 400000. In [3] it has been shown that for a slightly higher Reynoldsnumber of Re = 600000 a laminar separation bubble is formed close

to the leading edge upper surface with a severe impact on the **beginning** of the dynamic stall process.

Instantaneous flow measurements about an airfoil by particle image velocimetry (PIV) have been published in [4]. This non-intrusive diagnostic technique is able to measure **time accurate** velocity fields within a 2d laser-light sheet. The PIV-technique is therefore very suitable to measure complex highly unsteady flows as in the present dynamic stall cases. To the knowledge of the authors the ISL-measurements were the first PIV-application to flows under dynamic stall conditions in a windtunnel.

Due to the fact that unsteady separated flows with vortex shedding include strong reversed flow components the PIV-system has been further developed to include the possibility of image shifting by means of a rotating mirror in front of the camera, [4]. With this device a known constant velocity (corresponding to the rotation speed of the mirror) is added to the measured field thus obtaining velocity vectors which are all directed into the same mean direction. During postprocessing this artificially added constant velocity is again subtracted to give the final correct velocity field.

A complex and sophisticated postprocessing procedure [10] is applied to the PIV-images to get a final corrected velocity vector field.

Fig.8: Instantaneous velocity field measured by particle image velocimetry (PIV), with vorticity contours, left figures. Calculated vorticity contours (α = 24.69°↑), right figure.

NACA0012   rigid
$\alpha = 15° + 10° \sin \omega^* T$
$\omega^* = 0.3$, $Ma_\infty = 0.1$, $Re = 400000$

3.4 Results
a) Rigid airfoil.

Fig. 8 (left) shows a vector field measured by PIV about a rigid NACA0012 model at about $\alpha = 24°↑$. Below this figure the corresponding vorticity contours are displayed. The right hand figure shows vorticity contours evaluated from numerical data. At this instant of time the dynamic stall vortex has been developed and is moving along the airfoil upper surface. The vortex is still attached to the airfoil: lift- and moment-stall have not yet been started. The equivalence between measured and calculated vorticity contours is obvious. The velocity fields have been measured and plotted for a complete oscillatory cycle in incidence steps of 1°. From each vector plot the corresponding vorticity field has been calculated (one example is displayed in Fig.8). From these results a number of informations can be extracted which are important to understand the dynamic stall process:

1.   Up to $\alpha = 20°↑$ the flow is attached to the airfoil upper surface.

2.   For $\alpha > 20°$ a formation of the dynamic stall vortex starts at the leading edge.

α = 19.5°↓

NACA0012 rigid   NACA0012-0016 deforming

α = 15°↓
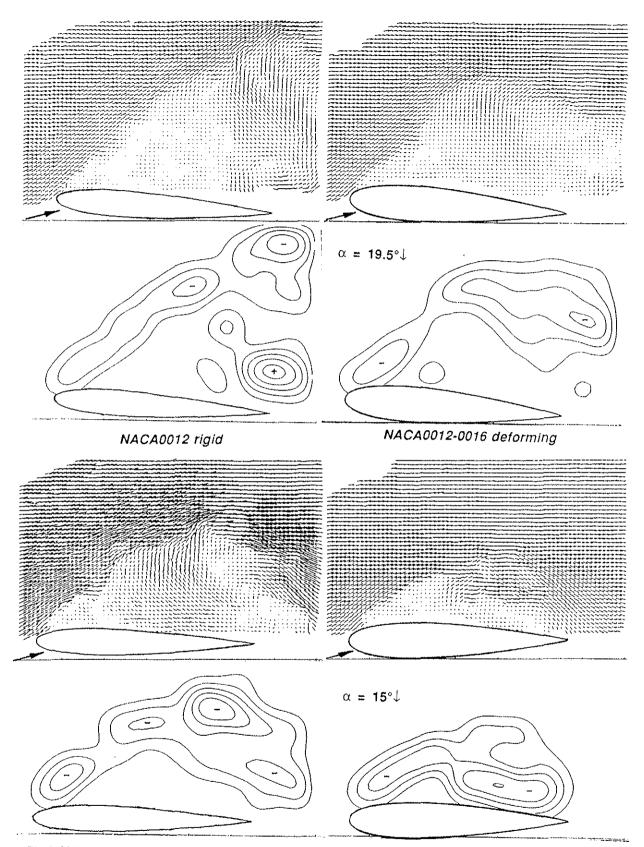
Fig.9: Velocity fields and vorticity contours during downstroke as measured by PIV.
Left: rigid airfoil
Right: deforming airfoil

3. The vortex moves along the airfoil upper surface and reaches midchord at about $\alpha = 24°\uparrow$ (Fig.8).

4. The primary vortex lifts off the surface (at about $\alpha_{max} = 25°$) and is shedded into the wake at the beginning of the downstroke movement.

5. Strong interaction occurs between the clockwise rotating leading edge vortex and a counter clockwise rotating vortex emanating from the trailing edge.

6. During the downstroke motion the area of strong vortex interaction is moving further downstream into the wake. During this phase the vorticity starting at the leading edge reattaches to the airfoil upper surface.

At later times during the oscillatory cycle. i.e. in the post-stall area, the PIV-data show remarkable *fluctuations* within the velocity vector fields: for this important information always four images have been taken at the same phase angle. The differences between these data are very small before the vortex shedding starts but they are severe in the post stall regime.

Due to this flow behavior during post stall (down stroke) it is concluded that the flow is very sensitive under separated conditions. Therefore it seems to be necessary to look into the details of only *one single cycle* instead of making ensemble averaging over a number of cycles. The averaging process (i.e. of pressure distributions) is smoothing out wiggles in the force and moment loops (see Fig.5) which are physically relevant.

The experimental results have also been compared with numerical data. The calculations show all the different features discussed above (see also Fig 8, right, as an example).

b) Deforming airfoil.

After successful application of the PIV-method on a rigid airfoil model during the dynamic stall event, the flexible model described in section 3.1 has been used for a first test under dynamic stall conditions. For these tests the compressed air inlets of the model were connected to the ISL pressure supply system. The airfoil deformation was controlled in such a way that the maximum thickness (approximately NACA0016, Fig 7) was obtained at the maximum incidence of $\alpha = 25°\uparrow$ during the oscillatory cycle.

It has been mentioned before that during these tests compressibility effects do not play an important role. But the airfoil deformation has other remarkable effects on the dynamic stall characteristics as has been shown in detail for the numerical data in section 2.

One important effect is the influence on the post-stall behavior of the unsteady flow. The calculated hysteresis loops of lift-, drag- and pitching moment (Fig.5) show a considerable reduction of the hysteresis area due to airfoil deformation. The flow reattaches at earlier times in the deformation cases. This behavior is also obvious for the experimental data

Fig. 9 shows measured velocity fields and the corresponding vorticity contours for two different time-instants during the down stroke motion of the airfoil at $\alpha = 19.5°\downarrow$ (upper figures) and at $\alpha = 15°\downarrow$ (lower figures). The left hand figures show results of the rigid model, the right hand figures display results of the deforming airfoil model. The region of flow separation is considerably reduced in the deforming case. The reattachment occurs at earlier times with strongly reduced vorticity shedding compared to the rigid case.

These experimental results look very promising for future investigation. It is planned to develop a test stand for oscillating models installed in a windtunnel facility operating in the more realistic Machnumber regime $0.2 \leq Ma_\infty \leq 0.4$ to also study compressibility effects.

4. Video movie

The numerical data of *case 1* have been prepared for a video movie to show several sequences of the deforming airfoil and comparisons with the rigid airfoil case. Vorticity-, pressure- and Machnumber-contours are displayed for the deforming airfoil in a space fixed frame of reference. The leading edge area is focused to show comparisons of these data for both the deforming and the rigid case in more detail. The medium video movie has proven to be an excellent tool to make the physics of the complicated unsteady flows better understandable. Focusing of interesting flow areas as well as slow motion sequences are easy achieved. The development of video movies will therefore be a guiding activity in future investigations

5. Conclusions.

For detailed investigations of flows under dynamic stall conditions a numerical method based on the time accurate solution of the Navier-Stokes equations as well as experimental non-intrusive instantaneous flow field measurements with particle image velocimetry (PIV) have been applied.

To favorably influence the dynamic stall numerical and experimental studies on *deforming* airfoils have been carried out. It has been shown that the influence of deformation on the dynamic stall process can be of considerable benefit. Future investigations are necessary and envisaged to study these problems in further details.

6. Acknowledgements.

7. References.

[1]	Ekaterinaris,J.A.	Compressibility Studies on Dynamic Stall 27th Aerospace Sciences Meeting. Jan. 9-12.1989.Reno,Nevada.
[2]	Geissler.W.	Instationäres Navier-Stokes Verfahren für beschleunigt bewegte Profile mit Ablösung. DLR-FB 92-03 (1992)
[3]	Carr,L.W. Chandrasekhara,M.S. Brock.N.J.	A Quantitative Study of Unsteady Compressible Flow on an Oscillating Airfoil. AIAA 22nd Fluid Dynamics & Lasers Conference. June 24-26,1991, Honolulu. Hawaii.
[4]	Raffel.M. Kompenhans.J.	PIV Measurements of unsteady transonic flowfields above a NACA0012 airfoil Laser Anemometry-Advances and Applications 5th International Conference, Veldhoven. The Netherlands. 23rd-27th August 1993.
[5]	Geissler,W. Vollmers.H.	Unsteady Separated Flows on Rotor Airfoils. -Analysis and Visualization of Numerical Data- 18th-European Rotorcraft Forum. Sept.15-18,1992.paper No.79. Avignon,France.
[6]	Carr,L.W. McAllister.K.W.	The Effect of a Leading-Edge Slat on the Dynamic Stall of an oscillating Airfoil. AIAA-paper 83-2533,Oct.1983.
[7]	McCloud.J.L. Hall,L.P. Brady,J.A.	Full-Scale Wind-Tunnel Tests of Blowing Boundary-Layer Control Applied to a Helicopter Rotor. NASA TN D-335,Sept.1960
[8]	Beam.R.W. Warming,R.F.	An Implicit Finite-Difference Algorithm for Hyperbolic Systems in Conservation-Law Form. J. of Comp Physics 22, 87-110 (1976).pp.87-100.
[9]	Wernert,P. Koerber,G. Wietrich.F.	A new experimental apperatus for the study of the unsteady flowfield over an airfoil in pitching and heaving motions using laser Doppler anemometry. Deutsch-Französisches Forschungsinstitut Saint-Louis (ISL) Bericht CO 229/92 (1992)
[10]	Raffel.M. Leitl,B. Kompenhans,J.	Data Validation for Particle Image Velocimetry. in: Application of Laser Techniques to Fluid Mechanics. 6th Int. Symposium. Lisbon 1992. Springer Verlag. Berlin 1992.